






## Theoretical study of the effect of lattice dynamics on the damping constant of FePt at finite temperature

Ivan Kurniawan <sup>1,2</sup>, Yoshio Miura <sup>1,3,\*</sup>, Guangzong Xing <sup>1</sup>, Terumasa Tadano <sup>1</sup>, and Kazuhiro Hono <sup>1,2</sup>

<sup>1</sup>Research Center for Magnetic and Spintronics Materials, National Institute for Materials Science (NIMS), 1-2-1 Sengen, Tsukuba 305-0047, Japan

<sup>2</sup>Graduate School of Science and Technology, University of Tsukuba, Tsukuba 305-8577, Japan

<sup>3</sup>Center for Spintronics Research Network (CSRN), Graduate School of Engineering Science, Osaka University, Machikaneyama 1-3, Toyonaka, Osaka 560-8531, Japan



(Received 17 December 2022; accepted 29 August 2023; published 15 September 2023)

Understanding magnetic damping behavior at finite temperatures is crucial for magnetization reversal, especially in heat-assisted magnetic recording (HAMR) media. In this paper, we calculate the intrinsic magnetic damping of  $L1_0$ -FePt, which is the prospective HAMR media, based on the Kamberský torque correlation model and the modified frozen thermal lattice disorder approach. Using the temperature-dependent scattering rate, the magnetic damping showed nonmonotonic behavior and slightly increased with increasing temperature, indicating that the lattice vibration enhances the interband transition around the Fermi level. Comparison of our results with the previous theoretical and experimental works clarified that, because the intrinsic damping of  $L1_0$ -FePt was always enhanced at high temperature, the reduction of the damping around the Curie temperature in the recent experiment emphasizes the importance of extrinsic contributions of damping for HAMR application.

DOI: [10.1103/PhysRevB.108.094426](https://doi.org/10.1103/PhysRevB.108.094426)

### I. INTRODUCTION

Magnetic damping constant  $\alpha$ , which represents the energy and spin-angular momentum dissipation rate of a local spin moment in magnetic systems, is a crucial parameter for magnetic storage and spintronics applications [1]. The critical current density of the spin-transfer torque (STT) switching in magnetic random-access memories is proportional to  $\alpha$ . Thus, low-damping material is required to enable magnetization switching with low energy consumption [2]. Furthermore, the voltage-controlled magnetic anisotropy switching also requires low magnetic damping for the reduction of write error rate during magnetization reversal [3]. Contrary to this, in magnetic recording technology such as heat-assisted magnetic recording (HAMR), high magnetic damping is preferred to improve the signal-to-noise ratio [4] and obtain a faster writing time [5], not only at ambient temperature but also at elevated temperatures characteristic to the writing process [6].

Here,  $L1_0$ -FePt nanogranular medium [7,8] was developed in response to the increasing demand for high areal density storage in the next generation of HAMR. It has large magnetocrystalline anisotropy ( $7 \times 10^7$  erg/cc) [9], which allows us to shrink and thermally stabilize the grains. Relatively low Curie temperature (750 K) [10] and large damping ( $\alpha > 0.05$ ) [11–14] are also beneficial for the easier writing process by heating the medium almost up to  $T_C$ . Therefore, understanding the temperature dependence of magnetic damping is essential to improve the switching properties of HAMR media. Unfortunately, the damping behavior of  $L1_0$ -FePt at finite temperature is still unclear, both from experimental and

theoretical points of view. In this paper, hopefully, we clarify this question in part.

Reported values of the experimentally measured magnetization damping coefficient vary significantly from one publication to another, even for the same material studied at room temperature. Mizukami *et al.* [11] reported the lowest effective Gilbert damping constant of 0.055 in  $L1_0$ -FePt epitaxial thin films, while Becker *et al.* [12] obtained  $\alpha = 0.1$  for the granular structure, and much larger values were also reported by Lee *et al.* [13] (0.2) and Kim *et al.* [14] (0.26). Note that, aside from the intrinsic damping contribution, measured damping also includes the equipment-dependent extrinsic damping component, which complicates the physical interpretation of the results [15].

On the other hand, the first-principles approach offers the intrinsic damping constant originating from the spin-orbit interaction (SOI) in magnetic systems [16–23]. Formulation of the intrinsic damping constant was proposed by Kamberský [16] based on the torque correlation model within the linear response theory, where the damping torque acting in the opposite direction to the STT comes from the magnetic friction between local moments and conduction electrons due to the SOI. By using the torque correlation model, Gilmore *et al.* [24] evaluated the damping constant for simple transition metals such as Fe, Co, and Ni and its dependence on the phenomenological parameter for the scattering rate  $\delta$ . Even with the semiempirical approach, their results agree well with the temperature dependence of experimental magnetic damping [25], demonstrating the indirect relation between the scattering rate parameter and temperature.

However, at high temperatures, spin fluctuation and atomic vibration effects become inevitably important in magnetic systems [26]. Therefore, including these effects will deepen

\*miura.yoshio@nims.go.jp

our understanding of the behavior of intrinsic damping at finite temperatures. Recently, unpredicted reduction of near- $T_C$  damping of FePt with temperature extracted from ferromagnetic resonance (FMR) linewidth measurement was reported by Richardson *et al.* [27]. This significant reduction may be disadvantageous for HAMR applications, especially leading to slower switching time and a smaller signal-to-noise ratio [6]. Recent theoretical works only consider spin fluctuation as the finite-temperature effect on the damping of FePt [28,29]. To calculate the damping, Hiramatsu *et al.* [29] treated the spin fluctuation in the framework of the disordered local moment (DLM) and included the small finite value of the impurity scattering rate  $\delta$  based on residual resistance representing temperature-independent scattering rate. It is found that the low-temperature damping value is significantly affected by these parameters, although its temperature dependence still qualitatively resembles the scattering rate dependence of magnetic damping of Fe at the ground state reported by Gilmore *et al.* [24]. This nonmonotonic behavior predicted by the torque correlation model can be explained by the fact that the scattering rate is somewhat enhanced by spin fluctuation at finite temperatures.

In contrast, the lattice dynamics effect via atomic vibrations on the FePt damping constant remains unclear. Previously, Liu *et al.* [30] introduced the so-called *frozen thermal lattice disorder* to incorporate atomic vibration into the damping calculation in the framework of the scattering theory. Since experimental FMR and phonon frequency are much smaller than the frequency corresponding to typical electronic Fermi velocity, the motion timescale can be separated and the electrons responsible for transport properties moved around the frozen phonons. The frozen phonon is expressed by shifting atomic position randomly and rigidly from the equilibrium coordinate following the Gaussian distribution of a particular value of the root-mean-square displacement, which is indirectly related to temperature. They found that the nonmonotonic behavior of damping in Fe, Co, and Ni can be reproduced by this simple model. However, they did not explicitly determine the atomic displacements at a given temperature, even though it could be done using phonon dispersion information. Hence, in this paper, we investigated the lattice dynamics effect on the damping constant of FePt at finite temperatures with the Kamberský torque correlation model and an improved frozen thermal lattice disorder approach.

## II. COMPUTATIONAL PROCEDURE

We performed first-principles density functional calculations using VASP [31] to obtain electronic structures and phonon dispersions of  $L1_0$ -FePt together with the projection onto local atomic orbitals. The projector augmented-wave potential was used to describe the behavior of core electrons [32]. The generalized gradient approximation proposed by Perdew, Burke, and Ernzerhof was adopted for the exchange and correlation energies [33]. A  $2 \times 2 \times 2$  supercell containing 8 Fe and 8 Pt atoms was constructed using the tetragonal unit cell with  $a = 5.4563 \text{ \AA}$  and  $c = 7.5579 \text{ \AA}$  for phonon and damping calculations. We used the plane-wave cutoff energy of 335 eV for the wave function expansion and  $10 \times 10 \times 10$   $k$ -points mesh for wave vector integration in the first Brillouin

zone. Note that the relatively sparse  $k$ -points mesh for damping calculations was used since the purpose of this paper is to offer insight into the temperature dependence of damping due to the atomic vibrations. We confirm that the qualitative feature of the scattering rate dependence of the damping constant has been converged by the present  $k$ -point density (see Fig. S1 in Supplemental Material S1 [34]).

The magnetic damping constant based on the torque correlation model can be described by the correlation function of the spin torque operator  $\eta^-$ :

$$\eta^- = [S^-, H_0] - \Omega S^- . \quad (1)$$

Here,  $S^-$  is the spin operator,  $\Omega$  is the frequency of uniform precession motions of local spin moments, and  $H_0$  is the Hamiltonian, which includes the usual spin-independent term, the ferromagnetic exchange potential, the SOI, and the potential deformation terms induced by finite-temperature effects such as lattice vibrations. The picture of the torque correlation model is closely related to the Brownian motion of particles in water, where the random collision of water molecules with particles leads to friction that affects the random motion of the particles. Analog to this model, local spin moments and conductive electrons in magnetic systems correspond to the particles and water molecules in Brownian motion, respectively. Thus, the generalized Langevin equation can be used to describe the spin dynamics:

$$\frac{dS^-(t)}{dt} = -i\Omega S^-(t) - i\eta^-(t) - \frac{1}{\mu_s} \int_0^t \langle [\eta^-(t'), \eta^+(t')] \rangle_0 S^-(t-t') dt' , \quad (2)$$

where the precession motion of local spin moments is described by the first term ( $-i\Omega S^-$ ), random spin-orbit torque from conductive electrons due to SOI by the second term ( $i\eta^-$ ), and damping motion by the last term. Here,  $\mu_s$  is the spin-magnetic moment, and  $\langle \dots \rangle_0$  indicates the thermal average for  $H_0$ . After implementing Laplace transform to solve this equation, we obtain the microscopic magnetic susceptibility as

$$\chi^+(\omega) = \frac{\mu_0(g\mu_B)^2}{\hbar V} \frac{-\mu_s}{\omega + i0 - \Omega + \Delta - \mu_s^{-1}F(\omega + i0)} , \quad (3)$$

where  $\Delta$ ,  $V$ , and  $g$  are the exchange splitting, unit-cell volume, and  $g$  factor of the present system, respectively. Here,  $F(\omega + i0)$  is the Green's function of the torque operator and represents the damping constant in its imaginary form:

$$F(\omega + i0) = -i \int_{-\infty}^{\infty} \langle [\eta^-(t'), \eta^+(t')] \rangle_0 \theta(t) \exp[i(\omega + i0)t] dt . \quad (4)$$

If we consider that the low-frequency limit of  $\Omega$  and the coupling between the spin moment and the potential deformation due to lattice vibrations are negligible as the first-order approximation, the torque operator in Eq. (1) is equivalent to the spin-orbit torque given by

$$\eta^- = \eta_0^- = [S^-, H_{SO}] , \quad (5)$$

where  $H_{SO} = \sum_I \xi_I \mathbf{L} \cdot \mathbf{S}$  is the spin-orbit Hamiltonian with  $\xi_I$  being the spin-orbit constant at the site  $I$ . Here,  $\mathbf{L} = (L_x, L_y, L_z)$  and  $\mathbf{S} = (S_x, S_y, S_z)$  are the orbital and spin-angular momentum operators, respectively.

The macroscopic approach for computing damping contribution can also be derived from the Landau-Lifshitz-Gilbert equation:

$$\frac{d\mathbf{M}}{dt} = -\gamma\mathbf{M} \times \mathbf{H}_{\text{eff}} + \alpha \frac{\mathbf{M}}{M_s} \times \frac{d\mathbf{M}}{dt}, \quad (6)$$

where the first term of Eq. (6) describes magnetization precession around the direction of external effective magnetic field  $\mathbf{H}_{\text{eff}}$ , and the second term represents the damping motion of local moment  $\mathbf{M}$ . Note that  $\alpha$ ,  $M_s$ , and  $\gamma$  correspond to the damping coefficient, saturation magnetization, and gyromagnetic ratio, respectively. By considering the precession of magnetization due to an external magnetic field  $\mathbf{H}_{\text{eff}}$  of the right-hand circular polarization, the susceptibility is expressed as

$$\chi^+(\omega) = -\frac{\gamma M_s}{\omega - \gamma H_{\text{eff}} + i\alpha\omega}. \quad (7)$$

Comparison between Eqs. (3) and (7) will give the expression of the damping constant as

$$\alpha = -\lim_{\omega \rightarrow 0} \frac{\gamma}{\hbar\mu_0 V M_s} \text{Im} \left[ \frac{1}{\omega} F(\omega + i0) \right]. \quad (8)$$

By evaluating the matrix elements of the spin-orbit torque operator for the wave function with SOI, the damping constant can be calculated via an *ab initio* method using the equation below:

$$\alpha = \frac{g}{\pi M_s} \sum_{\mathbf{k}} W_{\mathbf{k}} \sum_{m'} |\Gamma_{m'}^-(\mathbf{k})|^2 \times \frac{\delta}{(E_F - \varepsilon_{n\mathbf{k}})^2 + \delta^2} \frac{\delta}{(E_F - \varepsilon_{n'\mathbf{k}})^2 + \delta^2}, \quad (9)$$

where  $\Gamma_{m'}^-(\mathbf{k}) = \langle n, \mathbf{k} | [S^-, H_{\text{SO}}] | n', \mathbf{k} \rangle$  is a matrix element by wave vector  $\mathbf{k}$  between bands  $n$  and  $n'$  induced by the spin-orbit torque operator  $\eta_0^- = [S^-, H_{\text{SO}}] = \sum_l \xi_l (S^- L^z - S^z L^-)$ . These matrix elements are numerically integrated over all wave vectors  $\mathbf{k}$  with the weight of  $W_{\mathbf{k}}$  and band states together with electron spectral functions, which are Lorentzian centered at the band energy  $\varepsilon_{n\mathbf{k}}$  and broadened by the electron-lattice scattering rate  $\delta$ . Note that the band states  $|n, \mathbf{k}\rangle$ , Fermi energy  $E_F$ , and  $\varepsilon_{n\mathbf{k}}$  are easily obtained from the output of the *ab initio* calculations. In addition, we confirmed that using a larger supercell did not significantly affect the qualitative trend of the Lorentzian function; hence, the  $2 \times 2 \times 2$  supercell should be sufficient for the present calculation (see Fig. S2 in Supplemental Material S2 [34]).

Although we neglected the spin-phonon coupling in the correlation function of the spin torque, we incorporate the atomic vibration effect via phonon dispersion as *modified frozen thermal lattice disorder*, where the atomic displacement is explicitly determined from the phonon dispersion information. First, we confirmed that there is no negative phonon mode for the FePt structure calculated by PHONOPY [35], which implies the ground state is dynamically stable. The atomic displacements  $u_{\kappa\ell}^\beta$  in the supercell can be obtained from the normal mode coordinates ( $Q_{q\nu}$ ) in the reciprocal space as

$$u_{\kappa\ell}^\beta = \frac{1}{\sqrt{M_\kappa N_q}} \sum_{q\nu} Q_{q\nu} e_{\beta}(\kappa; \mathbf{q}\nu) \exp[i\mathbf{q} \cdot \mathbf{r}(\ell)], \quad (10)$$

where  $\beta$  is the Cartesian coordinate index,  $M_\kappa$  is the mass of the  $\kappa$ th atom in the unit cell,  $\ell$  is the unit cell index in the supercell, and  $N_q$  is the number of  $\mathbf{q}$  points commensurate with the supercell. The polarization vector  $e_{\beta}(\kappa; \mathbf{q}\nu)$  gives the direction in which each atom moves with the wave vector  $\mathbf{q}$  and the mode index  $\nu$ . To generate structural snapshots relevant at each temperature, we randomly sample  $Q_{q\nu}$  from the Gaussian (normal) distribution with the deviation  $\sigma_{q\nu}$ , which is given as [36]

$$\sigma_{q\nu}^2 = \langle Q_{q\nu} Q_{q\nu}^* \rangle = \frac{\hbar}{2\omega_{q\nu}} (2n_{q\nu} + 1), \quad (11)$$

where  $\omega_{q\nu}$  is the harmonic phonon frequency, and  $n_{q\nu}(\omega, T) = [\exp(\hbar\omega/k_B T) - 1]^{-1}$  being the Bose-Einstein occupation function. Therefore, we calculate the damping value of each snapshot using the Kambarský model and do averaging to obtain the damping value over hundreds of snapshots at each temperature. We confirmed that the averaging over 100 snapshots is enough to obtain the converged magnetic damping at finite temperatures up to 900 K.

The scattering rate  $\delta$  in Eq. (9) was estimated from the imaginary part of the Fan-Migdal (FM) self-energy defined as [37]

$$\Gamma_{n\mathbf{k}} = \text{Im} \Sigma_{n\mathbf{k}}^{\text{FM}}(\varepsilon_{n\mathbf{k}}) = \frac{\pi}{N_q} \sum_{m\mathbf{q}\nu} |g_{nm\nu}(\mathbf{k}, \mathbf{q})|^2 \times [(1 - f_{m\mathbf{k}+\mathbf{q}} + n_{q\nu})\delta(\varepsilon_{n\mathbf{k}} - \hbar\omega_{q\nu} - \varepsilon_{m\mathbf{k}+\mathbf{q}}) + (f_{m\mathbf{k}+\mathbf{q}} + n_{q\nu})\delta(\varepsilon_{n\mathbf{k}} + \hbar\omega_{q\nu} - \varepsilon_{m\mathbf{k}+\mathbf{q}})], \quad (12)$$

where  $g_{nm\nu}(\mathbf{k}, \mathbf{q})$  is the electron-phonon coupling constant and  $f_{n\mathbf{k}} = \{\exp[(\varepsilon_{n\mathbf{k}} - \mu)/k_B T] + 1\}^{-1}$  is the Fermi-Dirac distribution function. We used dense  $100 \times 100 \times 100$   $\mathbf{k}$ - and  $\mathbf{q}$ -point grids for the summation of Eq. (12). To that end, the electron-phonon coupling constants were first computed based on density functional perturbation theory (DFPT) for the  $2 \times 2 \times 2$   $\mathbf{q}$  points along with the  $12 \times 12 \times 12$   $\mathbf{k}$  points and subsequently interpolated to the dense grids using the Wannier interpolation. The DFT and DFPT calculations were performed under a collinear magnetic state using the QUANTUM ESPRESSO package [38], where the Garrity-Bennett-Rabe-Vanderbilt (GBRV) ultrasoft pseudopotentials [39] were used with the kinetic energy cutoffs of 90 and 1080 Ry, respectively, for the wave function and charge density. The maximally localized Wannier functions were constructed using the WANNIER90 code [40], where the outer energy window of  $[-10; 8]$  eV relative to the Fermi level was used. The calculation of  $\Gamma_{n\mathbf{k}}$  was performed using the PERTURBO code [41].

### III. RESULTS AND DISCUSSION

Before we include the finite-temperature effect in the damping calculation, we need to validate our calculation in the ground-state condition. It is known that the spectral shape of damping has a pattern like the density of states (DOS) around the Fermi level [16,24]. In Fig. 1, it is shown that our calculation for FePt maintains this similarity, suggesting that the main contribution to magnetization damping processes comes from electron states located near the Fermi level [Eq. (9)].

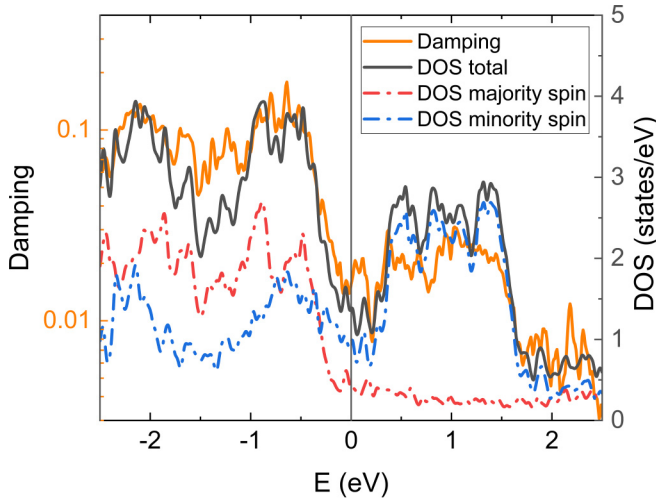


FIG. 1. The total damping and density of states (DOS; total, majority-spin, minority-spin) for  $L1_0$ -FePt at 0 K as a function of energy measured from the Fermi level. The left axis is the damping, and the right axis is the DOS.

The total intrinsic damping is the sum of the intraband and interband contributions. While the intraband contribution decreases with increasing the scattering rate (conductivitylike), the interband contribution is proportional to the scattering rate (resistivitylike) and dominates the total damping in the strongly scattered region. The difference in the scattering rate parameter  $\delta$  dependence between the intraband and interband contribution implicitly shows the nonmonotonic behavior of the temperature dependence of damping. Figure 2 demonstrates this behavior, where we confirm the good agreement in the qualitative trend previous calculation reported by Qu *et al.* [42].

In Fig. 3(a), we show the total damping computed with various scattering rates after averaging over 100 snapshots according to Eqs. (10) and (11) to include the effect of atomic vibrations for each temperature. It is found that the intraband and interband damping are dominantly contributed in the low and high scattering regions, respectively. However, the nearly

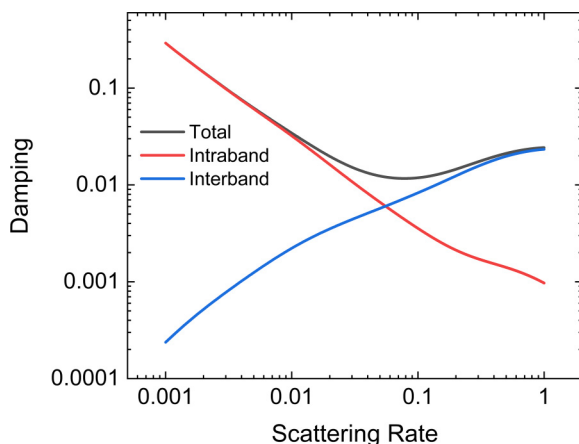


FIG. 2. The total, intraband, and interband damping dependence on the scattering rate parameter computed for  $L1_0$ -FePt at 0 K.

overlapped curve shown at elevated temperature (300–900 K) may imply that the effect of atomic vibrations on the magnetic damping is not significant, especially at high temperatures. Figure 3(b) contains the same information as Fig. 3(a) but shows the temperature dependence of damping using a constant scattering rate  $\delta$ . The range of the scattering rate  $\delta$  was chosen based on the values considered in the previous reports (0.0272–0.10 eV) [29,42]. When a relatively low scattering rate  $\delta = 0.03$ –0.04 eV is used, the temperature dependence of the damping value shows an approximately monotonic decrease followed by saturation of damping at high temperatures. However, the use of scattering rates  $\delta = 0.05$ –0.10 eV increases damping at high temperatures; hence, a nonmonotonic behavior is clearly demonstrated.

Since the results in Fig. 3 show that scattering rate plays an important role in the quantitative evaluation of the magnetic damping over the temperature range, we are motivated to evaluate the magnetic damping using calculated temperature-dependent scattering rates. To begin with, it is intuitive that the scattering rate increases at higher temperatures due to enhanced electron-phonon scatterings. Since the electron-phonon scattering gives the dominant contribution to the temperature dependence of the total scattering rate, we estimate  $\delta$  from the imaginary part of the FM self-energy [Eq. (12)]. In Fig. 4, we plot the calculated  $\delta$  values as a function of temperature  $T$ . Here, the calculated imaginary parts were averaged over the Kohn-Sham states in the range of  $E_F \pm 0.3$  eV because the bands around the Fermi level dominantly contribute to the damping. We confirmed that the averaged  $\delta$  value was not sensitive to the window energy when it is reasonably small, i.e.,  $\sim 0.05$ –0.5 eV. It is seen from Fig. 4 that the scattering rate  $\delta$  increases as the temperature rises, in accord with the aforementioned intuitive picture. The extrapolation of the  $\delta$  values gives a nonzero value at 0 K ( $\sim 0.007$  eV). Interestingly, this value is within the magnitude range of temperature-independent impurity scattering rate  $\delta$  estimated from residual resistivity by Hiramatsu *et al.* [29] (0.0027–0.027 eV).

Using the obtained imaginary part of the FM self-energy as the temperature-dependent scattering rate, we calculated the temperature dependence of damping. Since the spin fluctuation effect is excluded, there is no Curie temperature in this paper; hence, magnetization value is constant, and damping value up to 900 K can be obtained. However, it is important to note that the actual HAMR writing operation is carried out  $\sim 670$ –685 K (10–25 K below experimental Curie temperature), and our results show that the phonon excitation hardly affects the magnetic damping in this temperature range. In Fig. 5, the temperature dependence of damping due to the atomic vibration is shown by the red line-point together with the previous study of the temperature dependence of damping due to spin fluctuation reported by Hiramatsu *et al.* [29] (the black line-point). Our calculation shows a weak nonmonotonic behavior, which confirms that atomic vibration slightly enhances the high-temperature damping. However, this magnitude of the change in the damping due to atomic vibrations is not as large as the effect of spin fluctuation reported by Hiramatsu *et al.* [29]. This could be explained because the damping constant is inversely proportional to the magnetic moment, as shown in Eq. (9). Since the magnetization rapidly



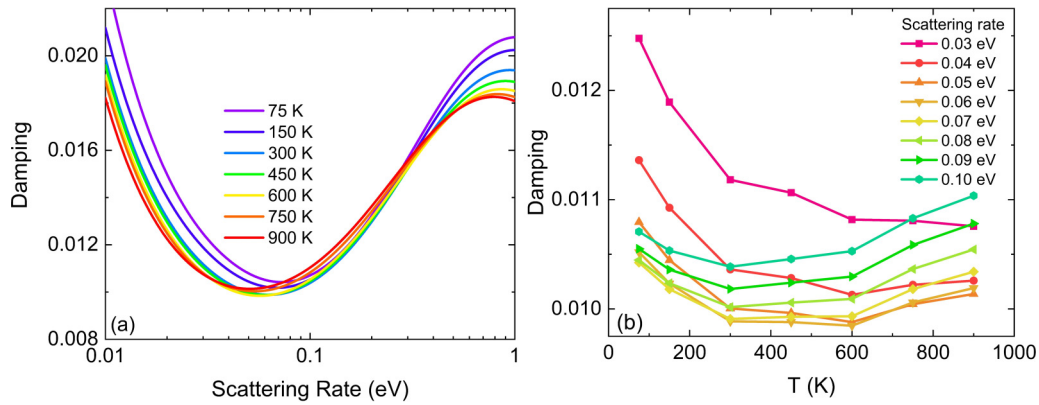


FIG. 3. (a) The scattering rate dependence of total damping with varying temperature. (b) The temperature dependence of total damping with varying scattering rate of  $L1_0$ -FePt.

decreases near the Curie temperature, the calculated damping due to the spin fluctuation will be drastically enhanced. On the other hand, we confirmed that the atomic vibration hardly affects the magnetization value even at high temperatures.

In Fig. 5, we also plot the reported experimental results of FePt damping taken from Refs. [27,43] by the blue and green line-points. In the experiment, they measure the FMR linewidth, which is directly proportional to the damping under the assumption of a negligible contribution of inhomogeneity line broadening. Thus, the damping value can be extracted from the FMR linewidth and plotted together with the calculated temperature dependence of damping. Previously, Richardson *et al.* [27] reported the reduction of the FMR linewidth in a  $L1_0$ -FePt granular sample, which correspond to the strong reduction of damping (blue dashed line). Since we and Hiramatsu *et al.* [29] separately reported that the intrinsic damping of FePt will increase at high temperatures due to the atomic vibration and spin fluctuation, respectively, we can rule out the intrinsic damping as an origin of the experimental reduction of the FMR linewidth (damping) observed by Richardson *et al.* [27]. Although the contributions from phonon excitation and spin fluctuation at finite temperatures are not additive in a quantitative manner, as shown by Ebert *et al.* [26], our results emphasize that the phonon

excitation effect is not detrimental for intrinsic damping at high temperatures, like with the spin-fluctuation effect in a qualitative manner [29]. In addition, in recently published work, Liu *et al.* [43] reported that the FMR linewidth of continuous thin films of cubic A1-FePt significantly increases near the Curie temperature (green dashed line). This qualitative behavior in cubic A1-FePt shows good agreement with the spin-fluctuation effect on damping of tetragonal  $L1_0$ -FePt reported by Hiramatsu *et al.* [29] due to the small extrinsic contribution. Note that the rapid increase of damping of A1-FePt reported by Liu *et al.* [43] happens at a lower temperature than that predicted by Hiramatsu *et al.* [29] for  $L1_0$ -FePt due to lower experimental  $T_C$  of A1-FePt (575 K) compared with the calculated  $T_C$  of  $L1_0$ -FePt using the DLM method (820 K) [29]. In addition, it is important to note that the DLM method

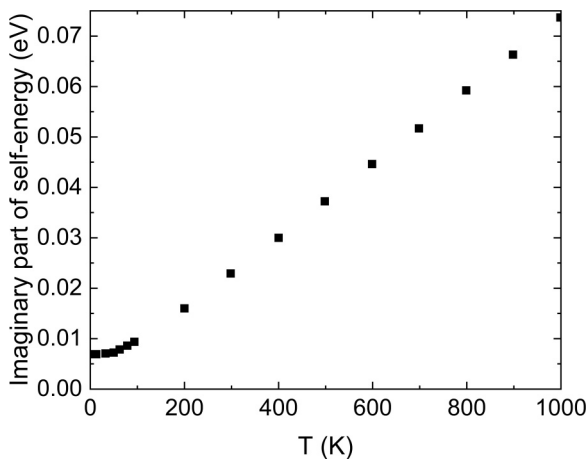


FIG. 4. Temperature dependence of  $\delta$  calculated from the imaginary part of the Fan-Migdal (FM) self-energy.

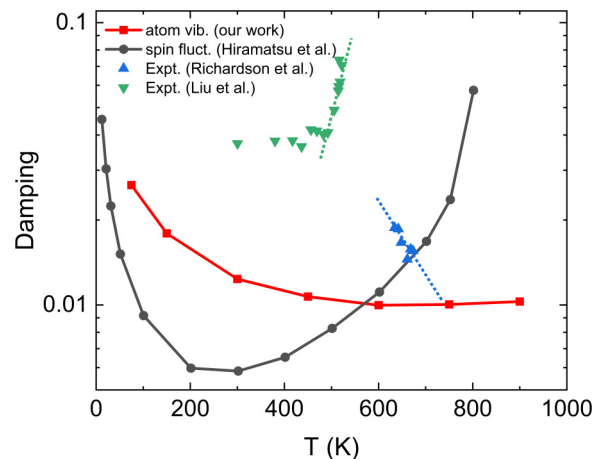


FIG. 5. Atomic vibration effect on the temperature dependence of the damping of  $L1_0$ -FePt calculated using the imaginary part of Fan-Migdal (FM) self-energy as temperature-dependent scattering rate. For comparison, the spin-fluctuation effect on the temperature dependence of damping constant of  $L1_0$ -FePt calculated by Hiramatsu *et al.* [29], experimental damping constant extracted from ferromagnetic resonance (FMR) linewidth of  $L1_0$ -FePt granular media by Richardson *et al.* [27], and A1-FePt continuous thin films by Liu *et al.* [43] are plotted together. Dashed line corresponds to the trend of the temperature dependence of experimental damping constant near the Curie temperature.

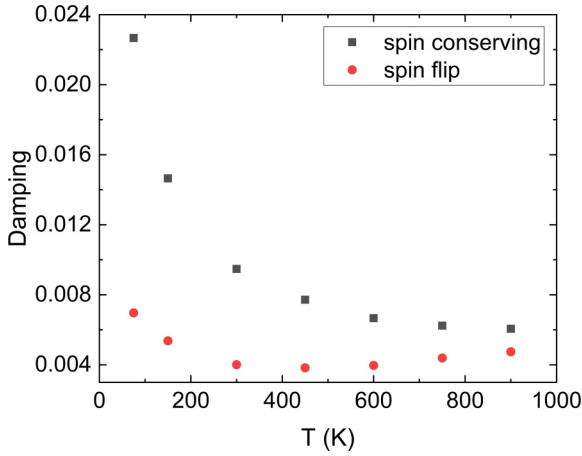


FIG. 6. Temperature dependence of the spin-conserving and spin-flip contribution to damping calculated using the imaginary part of Fan-Migdal (FM) self-energy as temperature-dependent scattering rate.

usually overestimates the Curie temperature, where the experimental  $T_C$  of  $L1_0$ -FePt is 695 K, as reported by Richardson *et al.* [27]. While the continuous Al-FePt thin films have fewer defects and smaller extrinsic contribution, the granular structure of  $L1_0$ -FePt media investigated by Richardson *et al.* [27] has more defects due to the grain boundary, resulting in the stronger extrinsic contribution to the damping [43]. Hence, the comparison of these results leads to two major findings: (1) the temperature dependence of intrinsic damping due to the atomic vibration and spin fluctuation is nonmonotonic, and the damping always increases with increasing the temperature near the Curie temperature; and (2) the extrinsic contribution will play an important role in the possible reduction of FePt damping in the experiment.

We split the spin-orbit torque operator  $\eta_0^- = [S^-, H_{SO}] = \sum_l \xi_l (S^- L^z - S^z L^-)$  into two parts: One is the spin-conserving term  $S^z L^-$ , and the other is the spin-flip term  $S^- L^z$ . In Fig. 6, we show separately the contributions of damping into spin-conserving transitions and spin-flip transitions using the calculated temperature-dependent  $\delta$  values. We found that the spin-conserving ( $S^z L^-$ ) contribution is much larger than the spin-flip ( $S^- L^z$ ) contribution. This can be attributed to two possible reasons. First, the small majority-spin DOS compared with the minority-spin DOS at the Fermi level due to the exchange splitting of FePt (see Fig. 1) will lead to the small contribution of the spin-flip transition from the occupied majority-spin states to the unoccupied minority-spin states. Second, the matrix elements of the spin flip  $\langle n, k | S^- L^z | n', k \rangle$  only allow the nonzero value for the six combinations of atomic orbitals with the same magnetic quantum numbers, where the spin conserving  $\langle n, k | S^z L^- | n', k \rangle$  give a nonzero value for the 16 combinations of atomic orbitals with different magnetic quantum numbers [44]. Note that different prerequisites for the nonzero values in spin-flip and spin-conserving matrix elements also provide justification to separately analyze the spin-flip and spin-conserving contributions to the total damping (see Fig. S3 in Supplemental Material S3 [34]). The temperature dependence of the two contributions is also different. The spin-conserving part of the damping shows a

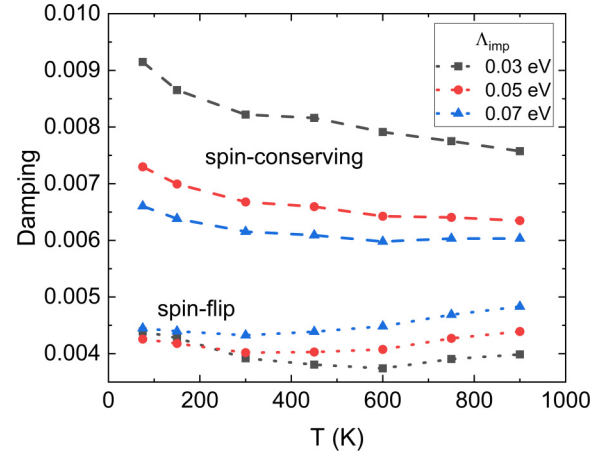


FIG. 7. Temperature dependence of damping by varied constant impurity scattering rate  $\Lambda_{\text{imp}}$ .

rather monotonic decrease. On the other hand, the spin-flip part shows more pronounced nonmonotonic behavior, which is like the total damping in Fig. 5. Previously, it was understood that nonmonotonic behavior of damping is attributed to the competition between the intraband (conductivitylike) and interband (resistivitylike) contribution. While the spin-flip term in the intraband contribution is almost negligible due to the assumption of a pure spin state, the strong spin-flip contribution from the interband transition may be the origin of the enhancement of damping at high temperatures.

It is difficult to obtain perfect samples experimentally due to introduction of impurities, formation of dislocations, etc. It is expected that low concentration of impurities does not affect the electronic structure and magnetic properties significantly. Therefore, we assumed that impurity concentration is proportional to the constant scattering rate due to impurities  $\Lambda_{\text{imp}}$ . In Fig. 7, we show the spin-conserving and spin-flip damping as a function of temperature for different impurity scattering rates  $\Lambda_{\text{imp}}$ . We found that the enhancement of the spin-flip damping at high temperatures is more pronounced with increasing  $\Lambda_{\text{imp}}$ . On the other hand, the spin-conserving damping hardly increases at high temperatures with increasing  $\Lambda_{\text{imp}}$ . This result implies that the presence of impurities in FePt may be beneficial by preventing undesirable damping coefficient reduction at high temperatures. Based on this simplified picture, impurities will act as local scattering centers which enhance the spin-flip transition process. However, this contribution can be less significant than spin fluctuation because the damping is explicitly dependent on the magnetization. Since the magnetic impurities having  $d$  orbitals may change the electronic structures of FePt and negatively impact the other important properties of HAMR such Curie temperature and anisotropy, nonmagnetic impurities without  $d$  orbitals such as carbon and boron can be considered possible candidates.

Finally, to understand how each phonon mode affects the damping behavior, we created modulated structures by displacing the atoms along the specified normal modes with different amplitudes at the commensurate  $\mathbf{q}$  points. The  $\kappa$ th atom displacements in the defined supercell with total  $N$

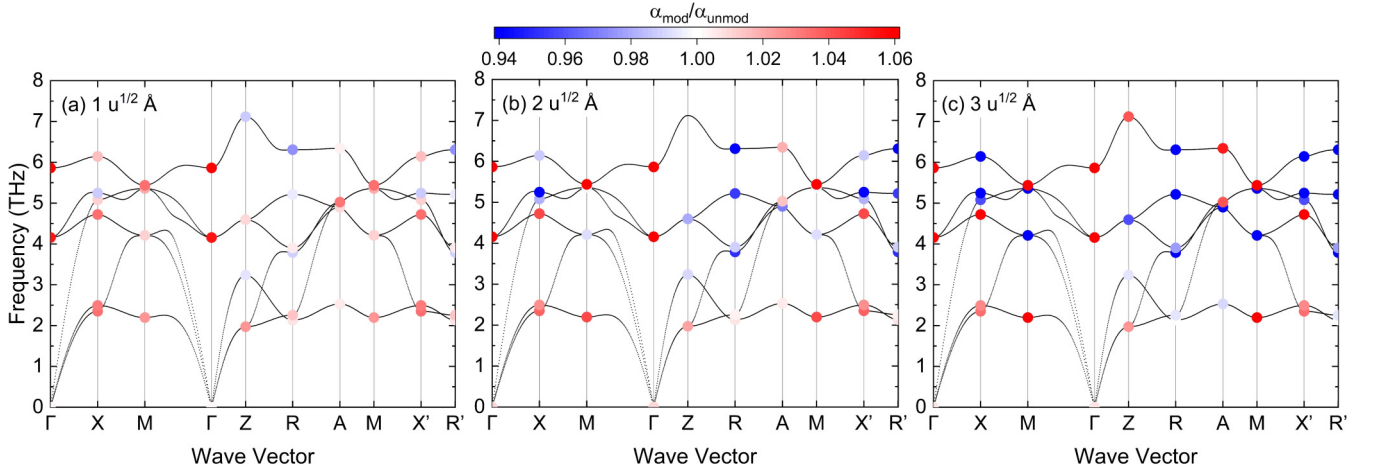


FIG. 8. (a)–(c) The mode-decomposed normalized damping  $\alpha_{\text{mod}}/\alpha_{\text{unmod}}$  of  $L1_0$ -FePt with amplitudes 1, 2, and  $3 u^{1/2} \text{ \AA}$  at constant scattering rate 0.05 eV, respectively.

atoms are defined as

$$\frac{A}{\sqrt{NM_\kappa}} \text{Re}[\exp(i\phi) e_\beta(\kappa; \mathbf{q}\nu) \exp(i\mathbf{q} \cdot \mathbf{r}_{\kappa\ell})], \quad (14)$$

where  $A$  is the amplitude in the unit of  $u^{1/2} \text{ \AA}$ , and  $\phi$  is the phase. We created supercells with displacements due to the phonon mode for each commensurate  $\mathbf{q}$  point. In the primitive  $L1_0$ -FePt unit cell, there are two atoms yielding six phonon modes at each  $\mathbf{q}$  point. Since the  $2 \times 2 \times 2$  supercell is used, there are eight different commensurate  $\mathbf{q}$  points labeled as follows:  $\Gamma (0,0,0)$ ,  $Z(0,0, \frac{1}{2})$ ,  $X(0, \frac{1}{2}, 0)$ ,  $R(0, \frac{1}{2}, \frac{1}{2})$ ,  $X'(\frac{1}{2}, 0, 0)$ ,

$R'(\frac{1}{2}, 0, \frac{1}{2})$ ,  $M(\frac{1}{2}, \frac{1}{2}, 0)$ , and  $A(\frac{1}{2}, \frac{1}{2}, \frac{1}{2})$ . Note that  $X(X')$  and  $R(R')$  are equivalent points in the phonon dispersion calculation.

In Figs. 8(a)–8(c), we show how each phonon mode affects the ratio of the damping in the modulated structure  $\alpha_{\text{mod}}$  to the damping in the unmodulated (perfect supercell) structure  $\alpha_{\text{unmod}}$  ( $\alpha_{\text{mod}}/\alpha_{\text{unmod}}$ ) with changing the amplitude of atomic displacements. The constant scattering rate of 0.05 eV was used. Red (blue) points correspond to the phonon mode that enhances (weakens) the damping value compared with the unmodulated structure. The presence of both red and blue phonon modes indicates two competing contributions to the

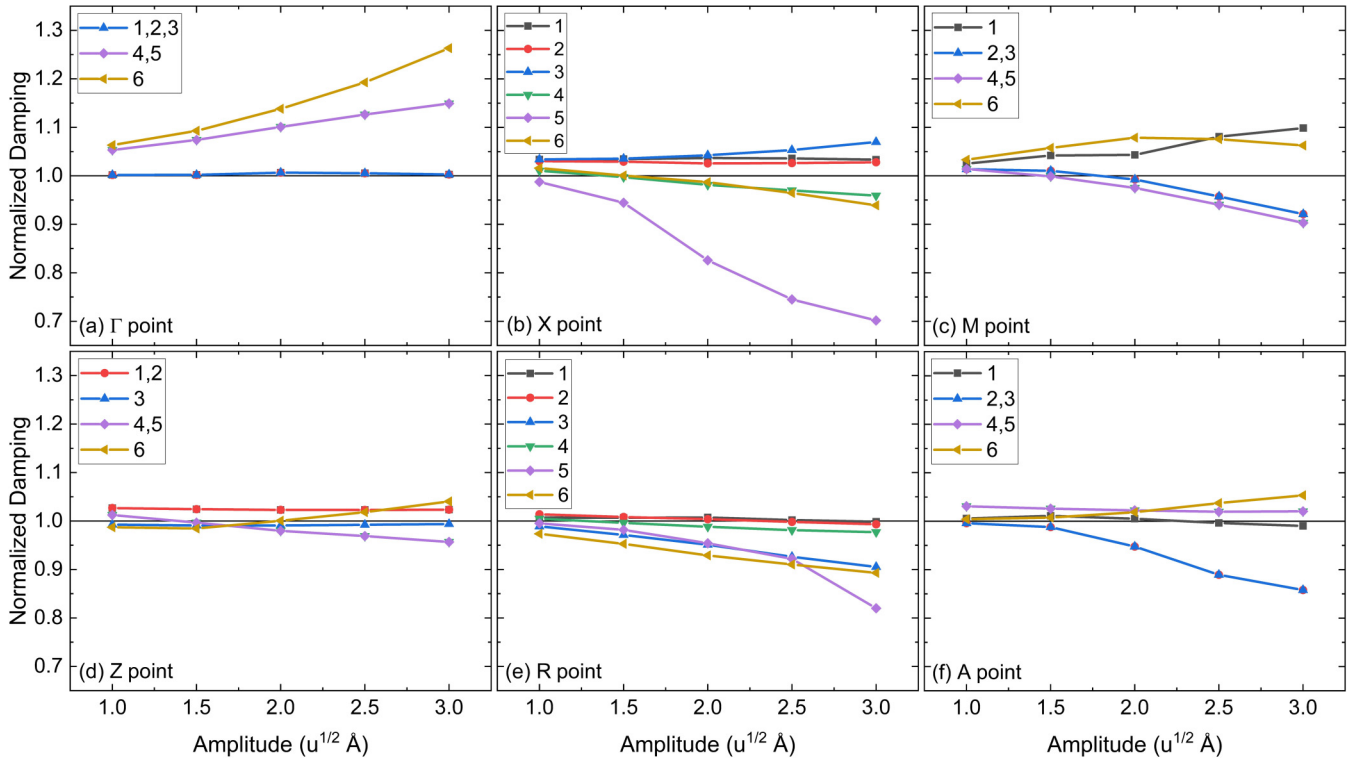


FIG. 9. (a)–(f) The amplitude dependence of normalized damping  $\alpha_{\text{mod}}/\alpha_{\text{unmod}}$  of  $L1_0$ -FePt due to phonon mode at  $\mathbf{q}$  point:  $\Gamma (0,0,0)$ ,  $X(0, \frac{1}{2}, 0)$ ,  $M(\frac{1}{2}, \frac{1}{2}, 0)$ ,  $Z(0,0, \frac{1}{2})$ ,  $R(0, \frac{1}{2}, \frac{1}{2})$ , and  $A(\frac{1}{2}, \frac{1}{2}, \frac{1}{2})$ , respectively. Every plot contained the contribution of each phonon mode indexed from lowest to highest frequency.

temperature dependence of damping, which may explain its nonmonotonic behavior.

At higher temperatures, a larger amplitude of displacements is expected, and higher-frequency phonon modes will be more occupied. We show in Figs. 9(a)–9(f) the amplitude dependence of the normalized damping  $\alpha_{\text{mod}}/\alpha_{\text{unmod}}$  of  $L1_0$ -FePt due to phonon modes at various commensurate  $q$  points. Larger amplitude and higher-frequency phonon mode generally result in a larger change in the magnitude of  $\alpha_{\text{mod}}/\alpha_{\text{unmod}}$ . The high-frequency phonon mode at the  $\Gamma$  point has always enhanced the damping, which may be a dominant contribution to the slight increase of damping at high temperatures due to the atomic vibration effect in Fig. 5.

#### IV. CONCLUSIONS

We carried out a theoretical study of the lattice dynamics effects on the damping constants of  $L1_0$ -FePt at finite temperatures based on the Kamberský torque correlation model and the improved frozen thermal lattice disorder approach. Using the imaginary part of the FM self-energy as the temperature-dependent scattering rate, we showed the weak nonmonotonic behavior of the temperature dependence of the damping. As a result, the damping slightly increases at high temperatures because of atomic vibrations, although the magnitude is not as large as that of the spin-fluctuation effect. Thus, our results rule out lattice dynamics as the exclusive origin of the observed temperature-induced decrease in the damping constant. The comparison with the reported experimental results emphasizes the importance of the extrinsic contribution to the

possible reduction of damping in  $L1_0$ -FePt granular media for HAMR application. Furthermore, we found that the increase of the damping at high temperatures is due to the spin-flip ( $S^-L^z$ ) contribution, which can be enhanced by the larger impurity scattering rate. These results suggest that, in practical applications, the inclusion of impurities such as carbon and boron may suppress the observed reduction in damping due to the extrinsic contribution at high temperature. Although the effect of lattice dynamics on the magnetic damping around the Curie temperature was not significant compared with the spin fluctuation, its effects will be more important for understanding the temperature dependence of the magnetic damping, if we include the spin-phonon coupling in the torque correlation model. In the future, we would like to consider spin-phonon coupling directly in the correlation function of the torque correlation model for intrinsic damping calculations.

#### ACKNOWLEDGMENTS

We are grateful to Y. Takahashi, Y. Sasaki, and K. Masuda of NIMS for valuable discussions on this paper. IK acknowledges NIMS for the provision of a NIMS junior research assistantship. This paper was partly supported by Grants-in-Aid for Scientific Research (Grants No. JP17H06152, No. JP20H00299, No. JP20H02190, and No. JP22H04966) from the Japan Society for the Promotion of Science, CSRN of Osaka University, and the Cooperative Research Project Program of the Research Institute of Electrical Communication in Tohoku University. The computations were performed on a Numerical Materials Simulator at NIMS.

- 
- [1] A. Hirohata, K. Yamada, Y. Nakatani, L. Prejbeanu, B. Diény, P. Pirro, and B. Hillebrands, *J. Magn. Magn. Mater.* **509**, 166711 (2020).
- [2] B. Diény and M. Chshiev, *Rev. Mod. Phys.* **89**, 025008 (2017).
- [3] Y. Shiota, T. Nozaki, S. Tamaru, K. Yakushiji, H. Kubota, A. Fukushima, S. Yuasa, and Y. Suzuki, *Appl. Phys. Express* **9**, 013001 (2016).
- [4] N. A. Natekar, Z. Liu, S. Hernandez, and R. H. Victora, *AIP Adv.* **8**, 056513 (2018).
- [5] R. Kikuchi, *J. Appl. Phys.* **27**, 1352 (1956).
- [6] M. Strungaru, S. Ruta, R. F. L. Evans, and R. W. Chantrell, *Phys. Rev. Appl.* **14**, 014077 (2020).
- [7] L. Zhang, Y. K. Takahashi, A. Perumal, and K. Hono, *J. Magn. Magn. Mater.* **322**, 2658 (2010).
- [8] D. Weller, G. Parker, O. Mosendz, A. Lyberatos, D. Mitin, N. Y. Safonova, and M. Albrecht, *J. Vac. Sci. Technol. B* **34**, 060801 (2016).
- [9] T. Shima, K. Takanashi, Y. K. Takahashi, and K. Hono, *Appl. Phys. Lett.* **81**, 1050 (2002).
- [10] A. Kußmann and G. G. v. Rittberg, *Int. J. Mater. Res.* **41**, 470 (1950).
- [11] S. Mizukami, S. Iihama, N. Inami, T. Hiratsuka, G. Kim, H. Naganuma, M. Oogane, and Y. Ando, *Appl. Phys. Lett.* **98**, 052501 (2011).
- [12] J. Becker, O. Mosendz, D. Weller, A. Kirilyuk, J. C. Maan, P. C. M. Christianen, T. Rasing, and A. Kimel, *Appl. Phys. Lett.* **104**, 152412 (2014).
- [13] K. D. Lee, H. S. Song, J. W. Kim, H. S. Ko, J. W. Sohn, B. G. Park, and S. C. Shin, *Appl. Phys. Express* **7**, 113004 (2014).
- [14] J. W. Kim, H. S. Song, J. W. Jeong, K. D. Lee, J. W. Sohn, T. Shima, and S. C. Shin, *Appl. Phys. Lett.* **98**, 092509 (2011).
- [15] Z. Xu, K. Zhang, and J. Li, *Phys. Rev. B* **104**, 224404 (2021).
- [16] V. Kamberský, *Czech. J. Phys.* **26**, 1366 (1976).
- [17] A. Sakuma, *J. Phys. Soc. Jpn.* **81**, 084701 (2012).
- [18] R. J. Elliott, *Phys. Rev.* **96**, 266 (1954).
- [19] Y. Yafet, *Solid State Phys.* **14**, 1 (1963).
- [20] P. Fulde and A. Luther, *Phys. Rev.* **175**, 337 (1968).
- [21] V. Korenman and R. E. Prange, *Phys. Rev. B* **6**, 2769 (1972).
- [22] F. Beuneu and P. Monod, *Phys. Rev. B* **18**, 2422 (1978).
- [23] A. Singh and Z. Teanović, *Phys. Rev. B* **39**, 7284 (1989).
- [24] K. Gilmore, Y. U. Idzerda, and M. D. Stiles, *Phys. Rev. Lett.* **99**, 027204 (2007).
- [25] S. M. Bhagat and P. Lubitz, *Phys. Rev. B* **10**, 179 (1974).
- [26] H. Ebert, S. Mankovsky, K. Chadova, S. Polesya, J. Minár, and D. Ködderitzsch, *Phys. Rev. B* **91**, 165132 (2015).
- [27] D. Richardson, S. Katz, J. Wang, Y. K. Takahashi, K. Srinivasan, A. Kalitsov, K. Hono, A. Ajan, and M. Mingzhong, *Phys. Rev. Appl.* **10**, 054046 (2018).
- [28] D. Ozaki, D. Miura, and A. Sakuma, *IEEE Trans. Magn.* **53**, 1 (2017).
- [29] R. Hiramatsu, D. Miura, and A. Sakuma, *Appl. Phys. Express* **15**, 013003 (2021).
- [30] Y. Liu, A. A. Starikov, Z. Yuan, and P. J. Kelly, *Phys. Rev. B* **84**, 014412 (2011).



- [31] G. Kresse and J. Furthmüller, *Phys. Rev. B* **54**, 11169 (1996).
- [32] P. E. Blöchl, *Phys. Rev. B* **50**, 17953 (1994).
- [33] J. P. Perdew, K. Burke, and M. Ernzerhof, *Phys. Rev. Lett.* **77**, 3865 (1996).
- [34] See Supplemental Material at <http://link.aps.org/supplemental/10.1103/PhysRevB.108.094426> for scattering rate dependence of damping with variation of number k points, estimation of temperature dependence of damping constant at  $4\times 4\times 4$  supercell, and contribution of cross-term.
- [35] A. Togo and I. Tanaka, *Scr. Mater.* **108**, 1 (2015).
- [36] Y. N. Wu, W. A. Saidi, J. K. Wuenschell, T. Tadano, P. Ohodnicki, B. Chorpening, and Y. Duan, *J. Phys. Chem. Lett.* **11**, 2518 (2020).
- [37] F. Giustino, *Rev. Mod. Phys.* **89**, 015003 (2017).
- [38] P. Giannozzi, O. Andreussi, T. Brumme, O. Bunau, M. B. Nardelli, M. Calandra, R. Car, C. Cavazzoni, D. Ceresoli, M. Cococcioni *et al.*, *J. Phys.: Condens. Matter* **29**, 465901 (2017).
- [39] K. F. Garrity, J. W. Bennett, K. M. Rabe, and D. Vanderbilt, *Comput. Mater. Sci.* **81**, 446 (2014).
- [40] G. Pizzi, V. Vitale, R. Arita, S. Blügel, F. Freimuth, G. Géranton, M. Gibertini, D. Gresch, C. Johnson, T. Koretsune *et al.*, *J. Phys.: Condens. Matter* **32**, 165902 (2020).
- [41] J.-J. Zhou, J. Park, I.-T. Lu, I. Maliyov, X. Tong, and M. Bernardi, *Comput. Phys. Commun.* **264**, 107970 (2021).
- [42] T. Qu and R. H. Victora, *Appl. Phys. Lett.* **106**, 072404 (2015).
- [43] C. Liu, K. Srinivasan, A. Ajan, E. McCollum, A. Kalitsov, V. Kalappattil, and M. Wu, *J. Magn. Magn. Mater.* **563**, 169988 (2022).
- [44] C. Liu, C. K. A. Mewes, M. Chshiev, T. Mewes, and W. H. Butler, *Appl. Phys. Lett.* **95**, 022509 (2009).